

Perception, Verdict, and Evolution: Hindsight-Driven Self-Refining Forensics Agent for AI-Generated Image Detection

Yangjun Wu, Keyu Yan, Yu Liu, Jingren Zhou, Fei Huang, Rong Zhang, Zhou Zhao, and Fei Wu

Abstract—The rapid advancement of generative models presents a significant challenge to existing deepfake detection methods, particularly given the widespread dissemination of highly realistic AI-generated images. Although Multimodal Large Language Models (MLLMs) show strong potential for this task, existing approaches suffer from two key limitations: insufficient sensitivity to fine-grained forensic artifacts and reliance on static synthetic supervision from frontier models, leading to limited flexibility and high-cost. To address these issues, we propose *ForeAgent*, an agentic forensics framework for AI-generated image detection with iterative self-evolution. First, *ForeAgent* adopts a Perception-Verdict architecture that aggregates multi-view cues spanning semantic, spatial, and frequency-domain features, and leverages an MLLM as a verdict module to fuse these signals for a logical-grounded verdict. Second, to enable continual self-improvement, we introduce a *Hindsight-Driven Self-Refining* strategy following a *Sampling-Reflection-Evolution* paradigm. The agent performs inference rollouts on training instances. Guided by ground-truth labels as hindsight, it reflects on failure cases and low-quality reasoning trajectories to regenerate higher-quality reasoning traces. These synthesized samples are then strictly filtered through a dual-expert quality gating module. *ForeAgent* continuously evolves via fine-tuning on self-curated high-quality samples. Extensive experiments demonstrate that *ForeAgent* achieves state-of-the-art performance on the Chameleon benchmark, reaching 82.18% accuracy (+16.41% over AIDE), and achieves 93.3% mean accuracy on AIGCDetect-Benchmark across 16 generators. In addition, external evaluation shows that *ForeAgent* produces more consistent and causally grounded reasoning compared to GPT-5 and GPT-5-mini.

Index Terms—AI-generated image detection, agentic forensics, Multimodal Large Language Models, self-refining.

I. INTRODUCTION

RECENT advances in generative models for image synthesis have significantly improved the visual fidelity of synthetic images, narrowing the perceptual gap between authentic and AI-generated content. Representative paradigms include Generative Adversarial Networks (GANs) [1], Diffusion Models [2], and Autoregressive Generation Models [3], [4]. The widespread dissemination of such content on social media platforms has raised substantial concerns in digital forensics [5] and copyright protection [6]. Consequently, reliable detection of AI-generated images has become a critical research problem for both academic study and real-world deployment.

Yangjun Wu, Zhou Zhao, and Fei Wu are with Zhejiang University, Zhejiang, China (e-mail: 12460105@zju.edu.cn; zhaozhou@zju.edu.cn; wufei@zju.edu.cn).

Yangjun Wu, Keyu Yan, Yu Liu, Jingren Zhou, Fei Huang and Rong Zhang are with Alibaba Group (e-mail: shuxin.wyj@alibaba-inc.com; yankeyu.yky@alibaba-inc.com; ly103369@alibaba-inc.com; jingren.zhou@alibaba-inc.com; feirhuang@gmail.com; stone.zhangr@alibaba-inc.com).

Yangjun Wu is the first author and the corresponding author.

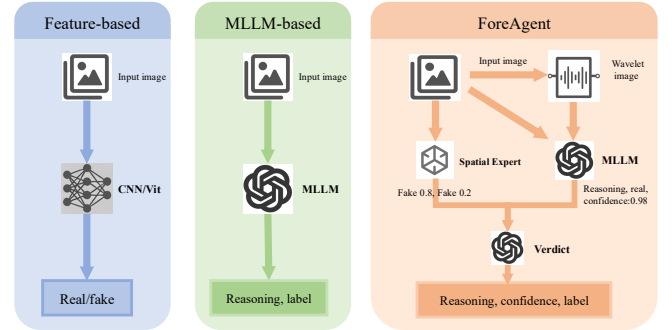


Fig. 1. Comparison of our method with feature-based and MLLM-based methods. Here, *reasoning* denotes the reasoning process.

Existing AI-generated image detection methods primarily fall into two categories: **Feature-based** detectors and **Multimodal Large Language Model MLLMs-based** explainable methods. Early feature-based approaches [7]–[13], such as NPR [12] and AIDE [13], focus on extracting statistical artifacts. For instance, NPR captures up-sampling traces by analyzing neighboring pixel relationships, while AIDE extracts frequency and semantic features to screen anomalies. However, these methods are typically pattern-matching schemes, lacking high-level semantic reasoning capabilities and cannot assess the intrinsic logical consistency of an image. The emergent capabilities of MLLMs have significantly advanced explainable AI-generated image detection [14]–[19]. For instance, AIGI-Holmes [18] leverages multiple SOTA multimodal models such as InternVL2.5-78B and Pixtral-124B [20] to synthesize reasoning outputs, which are subsequently refined through expert annotation. Similarly, FakeShield [21] exploits curated image editing pipelines in conjunction with GPT-4o [22] to generate fine-grained descriptions of tampered regions, manipulation content, and forensic traces. Despite these advances, current MLLM-based approaches suffer from two critical limitations: 1) while MLLMs demonstrate strong general visual understanding, they exhibit limited sensitivity to subtle artifacts and fine-grained anomalies characteristic of AI-generated imagery. 2) Existing methods heavily dependent on externally provided, static synthetic instruction data produced by models such as GPT-4o or Pixtral-124B, leaving the potential of reflective learning on misclassified samples and iterative self-refinement largely unexplored.

To address these limitations, we propose **ForeAgent**, an agentic forensic framework for AI-generated image detection built upon an iterative evolutionary strategy. The framework

integrates multi-perspective visual cues to enable comprehensive forensic analysis and evolves through a hindsight-driven self-refinement mechanism (guided by ground-truth labels), progressively improving both detection performance and interpretability. First, ForeAgent adopts a **Perception–Verdict** architecture to overcome the limitations of single-view detection. Unlike prior methods [18], [19] that modify backbone architectures by introducing dual-branch feature extractors (e.g., CNNs combined with MLLMs) and training task-specific classification heads, ForeAgent preserves the MLLM in its original form and leverages it as a centralized reasoning engine without architectural modification. Specifically, ForeAgent constructs a comprehensive perceptual input consisting of three complementary dimensions as depicted in Figure 1: (1) *Semantic cues* derived from the original image to capture high-level visual inconsistencies; (2) *Frequency-domain cues* obtained via *wavelet transforms* to expose spectral anomalies that are often imperceptible to human inspection. These two modalities are jointly provided to the MLLM as dual-image inputs; (3) *Spatial cues* extracted by invoking an external NPR (Neighboring Pixel Relationships) detector as a callable tool, which outputs structured inference results rather than raw feature maps. The MLLM further serves as a *verdict* module that integrates these multi-dimensional signals into a coherent and logically grounded decision, enabling holistic and evidence-aware forensic reasoning.

Second, to reduce reliance on external frontier MLLMs, image-editing or costly human annotations, we introduce a **Hindsight-Driven Self-Refining** strategy following a *Sampling–Reflection–Evolution* paradigm. During training, the agent performs inference rollouts to identify hard cases characterized by incorrect predictions or low-quality reasoning traces (details in supplemental materials). Guided by ground-truth labels as hindsight signals, the agent reflects on these failure cases and regenerates improved reasoning trajectories. The synthesized samples are subsequently filtered through a dual-expert quality-gating module. High-quality reasoning samples are used for supervised fine-tuning, whereas samples with correct predictions but suboptimal reasoning are retained for label-only supervision to preserve foundational knowledge. Through this iterative process, failure cases are transformed into high-value training signals, enabling continuous self-evolution of ForeAgent.

Our contributions are summarized as follows:

- (1) We propose ForeAgent, an agentic multi-view forensic framework that unifies semantic, spatial, and frequency-domain cues under a Perception–Verdict architecture without modifying the MLLM backbone.
- (2) We introduce a Hindsight-Driven Self-Refining paradigm that converts failure cases into high-value supervision signals through Sampling–Reflection–Evolution with dual-expert quality gating, enabling continual self-evolution.
- (3) Extensive experiments on AIGCDetectBenchmark and Chameleon demonstrate that ForeAgent achieves state-of-the-art performance and superior reasoning quality compared to GPT-5 and existing explainable detectors. The ForeAgent model will be publicly available at https://huggingface.co/Shimin/qwen3_vl_8b_foreagent

II. METHODOLOGY

In this section, we present **ForeAgent**, an agentic forensics framework for discerning authentic and synthetic images. The framework includes two core designs: (1) a *Perception–Verdict* architecture and (2) a *Hindsight-Driven Self-Refining* mechanism. The overview is illustrated in Figure 2.

A. Multi-view Cues Perception–Verdict

To overcome the limitations of single-view detection, ForeAgent adopts a *Perception–Verdict* architecture that aggregates multi-view cues spanning semantic, frequency-domain, and spatial dimensions. Rather than simply concatenating heterogeneous signals or training additional fusion modules, we employ an MLLM (Qwen3-VL-8B) as the central *reasoning agent*. The agent actively perceives semantic and frequency-domain cues through dual-image input, while invoking an external spatial expert (NPR detector [12]) as a callable tool to obtain spatial-domain evidence. A dedicated *Verdict* module then synthesizes these multi-dimensional findings, enabling the agent to produce a coherent, logically grounded, and fully interpretable detection conclusion.

1) *Multi-View Feature perception*: The input feature comprises: 1) Semantic cue (original image). This captures high-level visual inconsistencies and semantic artifacts that may indicate AI generation, such as unnatural object compositions, implausible lighting, or anomalous facial features. 2) Frequency-Domain cue (wavelet transform). We employ wavelet transformation to extract diagonal detail maps with fixed size (256,256), which expose frequency-domain anomalies that are often imperceptible in the pixel domain. 3) Spatial Cue (Optional). We employ the NPR detector [12] to capture structural traces left by up-sampling operations inherent in generative pipelines. In this study, we directly use this expert without tuning for simplicity.

The formulation of the standard detection task is that we have the image x and its related label y :

$$y = \Theta_{model}(x) \quad y \in \{\text{real}, \text{fake}\} \quad (1)$$

Θ refers to the learnable parameters. In our multi-view setting, ForeAgent feeds the original image x together with its frequency-domain counterpart x_{freq} as a joint (dual-image) input to the MLLM for semantic and spectral perception. Meanwhile, ForeAgent sends the original image x to the NPR expert and obtains its inference prediction. Thus, we revise the formulation as follows:

$$\mathbf{y}_1 = \mathcal{F}_{MLLM}(x, x_{freq}) \quad (2)$$

$$\mathbf{y}_2 = \mathcal{F}_{NPR}(x) \quad (3)$$

where $\mathbf{y}_1 = \{C_{conf}, R_{reasoning}, P_{pred}\}$ comprises the binary prediction $P_{pred} \in \{\text{real}, \text{fake}\}$, the confidence score $C_{conf} \in [0, 1]$, and the reasoning explanation $R_{reasoning}$ that provides interpretable justification for the decision. Simultaneously, the original image x is processed by spatial expert to extract low-level artifacts. $\mathbf{y}_2 = \{Pr_{real}, Pr_{fake}\}$ represents the probability distribution over real and fake classes.

This design enables ForeAgent to capture high-level semantic inconsistencies as well as frequency-domain artifacts

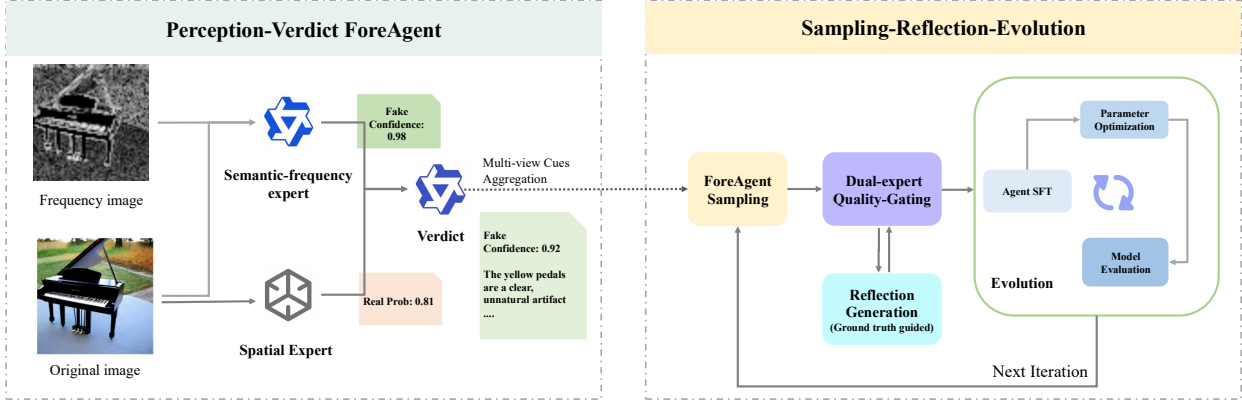


Fig. 2. **Overview of ForeAgent.** ForeAgent combines a multi-view *Perception–Verdict* architecture (left) with a *Hindsight-Driven Self-Refining* loop (right). A semantic–frequency expert and a spatial expert extract complementary cues, which a verdict module fuses into a confidence-calibrated verdict with interpretable rationale. Through iterative *Sampling–Reflection–Evolution*, the agent: (1) performs inference rollouts to collect predictions (*Sampling*); (2) reflects on failure cases guided by ground-truth labels to regenerate improved reasoning traces (*Reflection*); and (3) filters high-quality samples via dual-expert quality gating and fine-tunes itself for the next iteration (*Evolution*). This closed-loop paradigm enables continual self-improvement in AI-generated image detection.

via the MLLM , and low-level statistical fingerprints by the NPR expert, providing complementary evidence for discerning authentic and synthetic images.

2) *MLLM-Based Verdict*: The multi-view *evidence* obtained from different perspectives is fed into an MLLM-based *verdict module* (Qwen3-VL-8B as the backbone), which serves as the reasoning core of ForeAgent. Unlike conventional classifiers that directly output binary predictions from learned feature embeddings, our verdict module performs explicit logical arbitration over *inference-level signals* (i.e., perceptual findings and expert predictions) to render the final verdict. Specifically, the verdict module is prompted to:

- Inspect each view independently and summarize potential forgery indicators.
- Integrate and cross-check evidence across views to resolve conflicts and ambiguities.
- Produce a coherent rationale that culminates in a `Real` or `Fake` verdict with an associated confidence score.

The verdict module produces the final decision as:

$$\hat{y} = \mathcal{F}_{\text{MLLM}}(p, \mathbf{x}, \mathbf{x}_{\text{freq}}, \mathbf{y}_1, \mathbf{y}_2) \quad (4)$$

Formally, p is the system prompt (see supplemental materials verdict prompt), \hat{y} contains reasoning, prediction label v_{pred} and confidence. This design ensures holistic and evidence-based judgment, while providing interpretable reasoning traces aligned with the multi-view forensic evidence.

B. Hindsight-Driven Self-Refining

To reduce the reliance on external frontier MLLMs as well as costly human annotations, we introduce a Hindsight-Driven Self-Refining strategy. This mechanism allows ForeAgent to sample instances in the training set and perform targeted reflection on failure cases and low-quality outputs, thereby synthesizing higher-quality reasoning traces for iterative fine-tuning. The overall procedure follows a *Sampling–Reflection–Evolution* paradigm and the workflow of paradigm described in algorithm 1.

1) *Sampling*: We partition the training set into N disjoint shards $\{\mathcal{D}_i\}_{i=1}^N$ and perform iterative self-refinement over these shards. At iteration t , ForeAgent runs inference rollouts \hat{y} with the current agent $\pi_{\theta_{t-1}}$ on the selected shard \mathcal{D}_t and categorizes each trajectory into three groups: (1) *Incorrect Predictions*, where the predicted label v_{pred} differs from the ground-truth label v_{gt} . (2) *Low-Quality Reasoning*, where the prediction is correct ($v_{\text{pred}} = v_{\text{gt}}$) but the generated rationale \hat{R} is vague, generic, or logically flawed. (3) *High-Quality Reasoning*, where both the prediction is correct and the rationale is deemed evidence-grounded. The first two groups are treated as *hard cases* and are prioritized for the subsequent reflection stage, while the high-quality group can be retained as stable supervision.

2) *Dual-Expert Quality Gating (DEG)*: To ensure that the synthesized reasoning traces are both logically rigorous and evidentially grounded, we propose a multi-level dual-expert quality gating module. The module follows a “**le-nient entry, strict exit**” principle: a sample is *admitted* for reflection as long as *either* expert identifies any quality deficiency—specifically, when any of the following conditions is detected: logic consistent = false, evidence sufficient = false, causal clear = false, or quality score ≤ 4 . A sample is incorporated into the high-quality dataset $\mathcal{D}_{\text{high}}$ if and only if both experts agree that all quality criteria are satisfied.

Why Dual Experts? We employ two independent MLLMs as judges: ForeAgent (Qwen3-VL-8B) and *Qwen3-VL-Plus*. The rationale for adopting a dual-expert framework is empirically validated in our ablation study (Section III-C3), which demonstrates that the evaluation of dual-experts effectively mitigates bias of a single-model and significantly improves the reliability of the evaluation compared to approaches of a single-judge.

3) *Reflection*: The first two groups (*Incorrect Predictions* and *Low-Quality Reasoning*) are fed into a **Hindsight Reflection** process. Using the ground-truth label v_{gt} as hindsight, ForeAgent re-examines each original image x along with

Algorithm 1 Iterative Hindsight-Driven Self-Refining

Require: Training set \mathcal{D} , Test set \mathcal{D}_{test} , Initial model \mathcal{M}_{θ_0} , Maximum iterations T , Data splits N

Ensure: Refined model \mathcal{M}_{θ^*}

```

1: Initialize best score  $S_{best} \leftarrow 0$ , best model  $\theta^* \leftarrow \theta_0$ 
2: Partition  $\mathcal{D}$  into  $N$  subsets:  $\{\mathcal{D}_1, \mathcal{D}_2, \dots, \mathcal{D}_N\}$ 
3:
4: for  $t = 1$  to  $T$  do
5:   Select subset  $\mathcal{D}_t \leftarrow \mathcal{D}_{(t-1)}$ 
6:   Initialize refined sets:  $\mathcal{D}_{high} \leftarrow \emptyset, \mathcal{D}_{label} \leftarrow \emptyset$ 
7:
8:   Phase 1: Sampling and Quality Assessment
9:   Prediction:  $\hat{y} \leftarrow \pi_{\theta_{t-1}}(x)$ 
10:  Prediction label:  $v_{pred}$  from  $\hat{y}, v_{gt}$ 
11:  if  $v_{pred} = v_{gt}$  then
12:     $C_x = (x, \mathbf{x}_{freq}, \mathbf{y}_1, \mathbf{y}_2)$ 
13:    Evaluate quality:  $q \leftarrow \text{DEG}(C_x, \hat{y}, v_{gt})$ 
14:    if  $q$  is High then
15:       $\mathcal{D}_{high} \leftarrow \mathcal{D}_{high} \cup \{(x, \hat{y})\}$ 
16:    else
17:      Trigger reflection
18:    end if
19:  else
20:    Trigger reflection
21:  end if
22:
23:  Phase 2: Reflection with Dual-Expert Validation
24:  if Reflection triggered then
25:    Generate reflection candidates via ForeAgent:
26:     $tr_1 \leftarrow \text{Reflect}(x, \mathbf{x}_{freq}, \mathbf{y}_1, v_{gt})$  for perception  $y_1$ 
27:     $tr_2 \leftarrow \text{Reflect}(C_x, \hat{y}, v_{gt})$  for verdict  $\hat{y}$ 
28:    Evaluate candidates via DEG:
29:     $q_1 \leftarrow \text{DEG}(x, tr_1, v_{gt})$ 
30:     $q_2 \leftarrow \text{DEG}(C_x, tr_2, v_{gt})$ 
31:     $q = \max(q_1, q_2)$ 
32:    Appended to  $\mathcal{D}_{high}$  if  $q$  is High else  $\mathcal{D}_{label}$ 
33:  end if
34:
35:  Phase 3: Model Evolution and Evaluation
36:   $\theta_t \leftarrow \text{FineTune}(\theta_{t-1}, \mathcal{D}_{high} \cup \mathcal{D}_{label})$ 
37:   $S_t \leftarrow \text{Evaluate}(\mathcal{M}_{\theta_t}, \mathcal{D}_{test})$ 
38:  if  $S_t > S_{best}$  then
39:     $S_{best} \leftarrow S_t$ 
40:     $\theta^* \leftarrow \theta_t$ 
41:  else
42:     $\theta_t \leftarrow \theta^*$ 
43:  end if
44: end for
45:
46: return  $\mathcal{M}_{\theta^*}$ 

```

its frequency-domain counterpart \mathbf{x}_{freq} and regenerates two candidate corresponding reasoning traces tr_1 and tr_2 for perception (the system prompt can be found in Supplemental materials.): (1) For samples with incorrect predictions, the agent generates the corrected reasoning path tr_{corr} that leads to the correct verdict. (2) For samples with correct predictions but weak rationales, the agent refines the original output into an improved reasoning trace tr_{ref} with clearer logic and more concrete evidence. Both candidate traces are evaluated by the Dual-Expert Gating (DEG) module, yielding quality scores q_1 and q_2 . We select the candidate with the higher score, denoted as $q^* = \max(q_1, q_2)$; $tr^* = tr_{q^*}$, and check whether its quality meets a predefined threshold τ_t . The candidate is appended to \mathcal{D}_{high} only if $q^* \geq \tau_t$ and both experts agree on high quality;

otherwise, it is degraded to label-only supervision in \mathcal{D}_{label} .

To accommodate evolving learning dynamics, we adopt **adaptive quality thresholds** across iterations: thresholds are set relatively low in early stages to encourage exploration and capture diverse failure patterns, then progressively tightened in later iterations to ensure only high-quality reasoning is incorporated.

4) *Self-Improvement Evolution via Fine-Tuning.*: The synthesized reasoning samples undergo rigorous quality verification (described in Section II-B2) before being incorporated into the training set. The curated samples are classified into two types: (1) High-quality samples \mathcal{D}_{high} , which pass all verification criteria and are used with full reasoning supervision. (2) Label-only samples \mathcal{D}_{label} , which have correct labels but suboptimal reasoning quality and are degraded to label-only learning tasks.

These samples are then used to fine-tune the agent, enabling iterative self-evolution. After each training iteration, we evaluate the updated model θ_t on the test set \mathcal{D}_{test} . The model parameters are updated to the new checkpoint *if and only if* the performance S_t surpasses the previous best result S_{best} ; otherwise, the model reverts to the best-performing checkpoint from earlier iterations. This performance-gated update strategy ensures monotonic improvement and prevents model degradation. Through this process, ForeAgent effectively converts failure cases into high-value training signals, progressively sharpening its detection capability and reasoning quality across successive refinement cycles.

C. Training Pipeline

The overall training pipeline of ForeAgent consists of two phases:

a) *Phase 1: Foundational Pre-Training.*: We initialize the agent via supervised pre-training on a balanced dataset \mathcal{D}_{pre} containing authentic and AI-generated images. In this phase, each sample is annotated with a binary label (real or fake), and the model is trained with cross-entropy loss. This stage establishes fundamental discriminative capabilities without reasoning supervision.

b) *Phase 2: Iterative Self-Refinement.*: The agent undergoes multiple iterations of the **Sampling-Reflection-Evolution** loop. In each iteration t , ForeAgent first samples and reflects on its failure cases to generate improved reasoning traces. The quality-gated samples are then used to LoRA fine-tune the agent, after which the adapter weights are merged into the base model to obtain the updated agent $\pi_{\theta_{t+1}}$.

We evaluate the updated model on the test set. If the performance improves compared to the previous iteration, the new parameters are retained and the loop proceeds to the next iteration. Otherwise, we revert to the previous checkpoint π_{θ_t} and continue. The iterative process terminates when the maximum number of iterations T_{max} (Default 5) is reached.

Through this hindsight-driven self-refining mechanism, ForeAgent achieves continuous self-evolution, progressively improving both detection accuracy and interpretability without requiring additional human annotations or reliance on proprietary frontier models.

TABLE I
RESULTS ON AIGCDETECTBENCHMARK. WE REPORT PER-GENERATOR ACCURACY (%) AND THE MEAN ACCURACY ACROSS ALL GENERATORS.

Model	ProGAN	StyleGAN	BigGAN	CycleGAN	StarGAN	GauGAN	StyleGAN2	WFIR	ADM	GLIDE	Midjourney	SD1.4	SD1.5	VQDM	Wukong	DALLE2	Mean
CNNSpot	100.0	90.2	71.2	87.6	94.6	81.4	86.9	91.7	60.4	58.1	51.4	50.6	50.5	56.5	51.0	50.5	70.8
FreDet	99.4	78.0	82.0	78.8	94.6	80.6	66.2	50.8	63.4	54.1	45.9	38.8	39.2	77.8	40.3	34.7	64.0
Fusing	100.0	85.2	77.4	87.0	97.0	77.0	83.3	66.8	49.0	57.2	52.2	51.0	51.4	55.1	51.7	52.8	68.4
LNP	99.7	91.8	77.8	84.1	99.9	75.4	94.6	70.9	84.7	80.5	65.6	85.6	85.7	74.5	82.1	88.8	83.8
LGrad	99.8	91.1	85.6	86.9	99.3	78.5	85.3	55.7	67.2	66.1	65.4	63.0	63.7	73.0	59.6	65.5	75.3
UnivFD	99.8	84.9	95.1	98.3	95.8	99.5	75.0	86.9	66.9	62.5	56.1	63.7	63.5	85.3	70.9	50.8	78.4
DIRE-G	95.2	83.0	70.1	74.2	95.5	67.8	75.3	58.1	75.8	71.8	58.0	49.7	49.8	53.7	54.5	66.5	68.7
DIRE-D	52.8	51.3	49.7	49.6	46.7	51.2	51.7	53.3	98.3	92.4	89.5	91.2	91.6	91.9	90.9	92.5	71.5
PatchCraft	100.0	92.8	95.8	70.2	100.0	71.6	89.6	85.8	82.2	83.8	90.1	95.4	95.3	88.9	91.1	96.6	89.3
NPR	99.8	97.7	84.4	96.1	99.4	82.5	98.4	65.8	69.7	78.4	77.9	78.6	78.9	78.1	76.1	64.9	82.9
AIDE	100.0	99.6	84.0	98.5	99.9	73.3	98.0	94.2	93.4	95.1	77.2	93.0	92.9	95.2	93.6	96.6	92.8
Qwen3-VL-8B	72.1	51.0	53.4	61.0	53.6	58.5	50.1	50.0	52.3	55.8	51.7	52.4	52.5	54.6	57.2	51.9	54.9
Qwen3-VL-32B	79.4	52.6	57.7	73.4	75.5	71.7	51.0	54.0	56.9	62.9	55.8	55.1	55.1	59.4	62.9	52.8	61.0
AIGI-Holmes	100.0	98.4	94.5	97.0	100.0	95.2	98.9	95.7	88.4	91.5	81.6	91.3	91.4	90.9	89.5	85.3	93.2
ForeAgent	99.9	98.2	83.1	96.1	99.9	80.5	99.7	63.4	91.5	97.0	96.0	98.3	98.2	95.6	97.1	98.9	93.3

III. EXPERIMENTS

A. Experimental Settings

1) *Detector baselines.*: For a fair comparison, we perform comparisons of our approach with existing state-of-the-art featured-based detectors, including CNNSpot [8], FreDet [9], Fusing [23], LNP [24], LGrad [25], Dire [26], UnivFD [27], PatchCraft [28], NPR [12], AIDE [13] and Effort [11]. Meanwhile, we also choose popular open-sourced MLLMs, comprising AIGI-Holmes [18], Qwen3-VL-8B-Instruct, Qwen3-VL-32B-Instruct [29], Llama-3.2-11B-Vision-Instruct, and Proprietary Models GPT5-mini and GPT5.

2) *Datasets.*: We conduct experiments on two benchmarks under different training set to ensure fair comparison with prior work. First, following the standard setting adopted in previous studies [8], [12], [24], [26], [27], all methods are trained exclusively on four object categories (*car*, *cat*, *chair*, *horse*) generated by ProGAN [10] and evaluated on AIGCdetectBenchmark [28], which spans 16 diverse generators. This setting assesses cross-generator generalization under a unified training regime. Second, we randomly sample both 60,000 real/fake images from the Genimage [30] training split to perform foundational pre-training. Subsequently, we apply the proposed *Hindsight-Driven Self-Refining* strategy on an additional 100,000 training samples, enabling iterative self-evolution through the *Sampling-Reflection-Evolution* loop. Finally, ForeAgent is evaluated on the Chameleon set [13] to verify detection performance.

3) *Implementation Details.*: We adopt Qwen3-VL-8B-Instruct as the backbone without architectural modification for our agent. During the foundation LoRA pre-training phase, we utilize the AdamW optimizer with a learning rate of 5×10^{-6} , setting the LoRA rank to 64 and alpha to 128. In the subsequent self-evolution phase, we configure the number of candidate generations to 2 with a sampling temperature of 0.9, and adjust the learning rate to 1×10^{-6} . The ForeAgent is trained on 8 NVIDIA A100 GPUs, with the training duration set to 2 epochs for the pre-training stage and 1 epoch for the self-evolution stage, respectively. We treat NPR as an external tool (without any parameter updates) and integrate its predictions into the MLLM via tool calling. Following standard protocols in AI-generated content detection, we evaluate our method using classification accuracy for real and fake samples.

B. Experimental Results

1) *Results On AIGCdetectBenchmark*: Table I summarizes the per-generator accuracy across 16 generators. Overall, **ForeAgent** achieves the highest mean accuracy of **93.3%**, slightly outperforming the strongest baselines AIGI-Holmes (93.2%) and AIDE (92.8%). Notably, ForeAgent demonstrates clear advantages on modern diffusion-based generators. For instance, it achieves 96.0% on Midjourney (vs. 81.6% for AIGI-Holmes and 77.2% for AIDE), 98.9% on DALLE2 (vs. 85.3% and 96.6%), and 98.3%/98.2% on Stable Diffusion v1.4/v1.5 (vs. 91.3%/91.4% and 93.0%/92.9%), consistently surpassing both leading baselines by significant margins. Similarly strong results are observed on GLIDE (97.0%), Wukong (97.1%), and VQDM (95.6%), indicating robust generalization to contemporary AIGC pipelines. In contrast, open-source MLLM baselines without forensic-specific design (Qwen3-VL-8B/32B) lag behind substantially (54.9% and 61.0% mean), confirming that generic visual understanding alone is insufficient for fine-grained AIGC forensics. We note that ForeAgent is less competitive on WFIR (63.4%), where several traditional CNN-based detectors (*e.g.*, CNNSpot at 91.7%, AIDE at 94.2%) perform considerably better, suggesting that certain sources with distinct post-processing or domain-specific characteristics remain challenging and may benefit from further source-aware augmentation or improved spatial-frequency fusion strategies.

2) *Results On Chameleon*: Table II reports per-class and overall accuracy on Chameleon. Classical forensic detectors (Dire, PatchCraft, and NPR) achieve near-perfect accuracy on real images ($\geq 96.5\%$) but fail on fake images ($\leq 2.1\%$), indicating limited robustness to highly realistic AI-generated content. UnivFD and effort exhibit the opposite bias, performing substantially better on fake images ($\sim 85.5\%$) while sacrificing real-image accuracy ($\sim 41.6\%$), which leads to only moderate overall performance ($\sim 60.4\text{--}60.7\%$).

Among MLLM baselines, open-source vision-language models (*e.g.*, Qwen3-VL-8B/32B and Llama-3.2-11B-Vision) generally show strong recognition of real images but struggle to detect fakes, resulting in overall accuracy below 63%. AIDE improves the overall score to 65.77%, yet its fake accuracy remains limited (26.80%), suggesting that scaling explainable detection still requires stronger artifact sensitivity and more reliable reasoning.

ForeAgent achieves the best overall accuracy (**82.18%**), slightly improving real-image accuracy compared to GPT5

TABLE II

COMPARISON ON CHAMELEON. WE REPORT ACCURACY(%) FOR REAL, FAKE, AND OVERALL IMAGE DETECTION. THE BEST AND SECOND-BEST RESULTS ARE HIGHLIGHTED IN **BOLD**, UNDERLINED, RESPECTIVELY.

Method	Real	Fake	Overall
<i>Feature-based Forensic Methods</i>			
Dire	99.73	2.09	57.83
PatchCraft	96.52	1.39	55.70
NPR	100.00	1.68	57.81
UnivFD	41.56	85.52	60.42
AIDE	95.06	26.80	65.77
Effort	41.66	85.92	60.65
<i>MLLM-based Methods</i>			
Qwen3-VL-8B-Instruct	98.67	10.03	60.63
Qwen3-VL-32B-Instruct	96.96	17.79	62.33
Llama-3.2-11B-Vision-Instruct	76.23	28.15	55.59
AIGI-Holmes (7B)	-	-	75.90
GPT-5-mini	94.40	36.71	69.65
GPT-5	92.74	<u>67.50</u>	<u>81.91</u>
ForeAgent (Ours)	<u>96.69</u>	61.86	82.18

(96.69% vs. 92.74%) while maintaining competitive fake-image accuracy (61.86%). Compared with AIDE, ForeAgent yields a substantial gain in overall accuracy (+16.41%), demonstrating the effectiveness of combining multi-view forensic cues with hindsight-driven self-refinement. Notably, ForeAgent approaches GPT5 in fake detection while outperforming it in overall accuracy, indicating improved robustness under class imbalance and reduced bias toward either real or fake classes.

TABLE III

THE COMPARISON OF REASONING QUALITY SCORE (RATED 0-10).

Model	AVG Score
GPT5-mini	4.81
GPT5	4.15
ForeAgent	5.35

3) *Reasoning quality evaluation*: To evaluate the quality of reasoning generated by different models, we randomly sample 2,000 instances from the prediction file generated by GPT5 on AIGCDetectBenchmark, and employ Gemini-3-flash-preview as an external judge. We assess reasoning quality across four dimensions: *quality_score* (Rated 0-10), *logic_consistent* (logical coherence), *evidence_sufficient* (adequacy of supporting evidence), and *causal_clear* (clarity of causal reasoning). The evaluation results are summarized in Table III, Figure 3.

Table III presents a comparison of reasoning quality across different models. Notably, GPT5-mini (4.81) surpasses GPT5 (4.15), indicating that model scale alone does not guarantee superior reasoning quality. Our proposed ForeAgent achieves the highest overall score (**5.35**), outperforming both baseline models by a substantial margin. This improvement demonstrates that ForeAgent’s self-evolution paradigm effectively enables adaptive calibration of reasoning depth, leading to more robust and balanced performance.

TABLE IV

COMPARISON ON CHAMELEON. WE EVALUATE SFT, FOREAGENT WITHOUT NPR, AND THE FOUR THE DISCRETE WAVELET TRANSFORM: APPROXIMATION (cA), HORIZONTAL DETAIL (cH), VERTICAL DETAIL (cV), AND DIAGONAL DETAIL (cD). (%)

Wavelet Type	Real	Fake	Overall
Qwen3-VL-8B-SFT	54.69	77.32	64.40
+ cA (Approximation)	50.68	88.69	66.99
+ cH (Horizontal)	31.85	91.36	57.38
+ cV (Vertical)	50.67	85.77	65.73
+ cD (Diagonal)	86.37	53.19	72.13
ForeAgent wo NPR	96.12	41.65	72.41
ForeAgent (full)	95.26	43.46	73.03

Figure 3 shows that GPT5-mini achieves lower logical consistency (65.0%), suggesting it excels on *easy* samples with clear artifacts yet struggles with *hard* cases involving subtle cues. Conversely, GPT5 demonstrates stronger logical consistency (73.5%), reflecting a tendency toward hedged, moderate-quality reasoning that prioritizes stability over decisiveness. ForeAgent benefits from hindsight-driven self-refinement, which attains the strongest average pass rates on *logical consistency* (75.6%) and *causal clarity* (76.1%), while maintaining competitive *evidence sufficiency* (38.4%) compared to GPT5-mini.

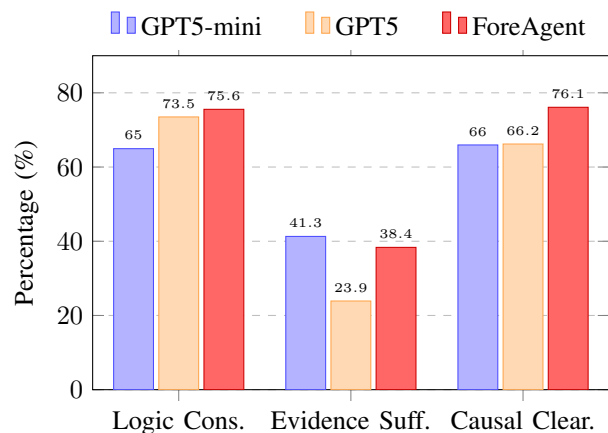


Fig. 3. Comparison of reasoning quality metrics. While GPT5-mini excels in evidence and GPT5 in logic, **ForeAgent** achieves the best balance, leading in Logical Consistency and Causal Clarity.

C. Ablation study

1) *Effect of Wavelet Decomposition Components and NPR.*: To investigate which sub-band from the discrete wavelet transform (DWT) provides the most discriminative frequency-domain cues for AI-generated image detection, we conduct a systematic comparison across four wavelet components. All experiments use Qwen3-VL-8B with LoRA fine-tuning (rank=64, alpha=128) on 120K training samples from the GenImage. As shown in Table IV, the four sub-bands are defined as follows: **cA (Approximation)**: Low-frequency coefficients that preserve the coarse structure and global content of the image. **cH (Horizontal)**: Horizontal detail coefficients that

capture vertical edges and horizontal texture variations. **cV (Vertical)**: Vertical detail coefficients that capture horizontal edges and vertical texture variations. **cD (Diagonal)**: Diagonal detail coefficients that capture diagonal edges and oblique texture patterns.

Sub-band selection. cD yields the highest overall accuracy (72.13%), substantially outperforming cA (66.99%), cV (65.73%), and cH (57.38%). It also achieves the most balanced performance between real and fake classes (86.37% vs. 53.19%), whereas other sub-bands exhibit pronounced bias toward the fake class. We attribute this to the fact that modern generative pipelines often employ convolutional up-sampling operations that introduce characteristic artifacts—such as checkerboard patterns and irregular edge transitions—predominantly along diagonal orientations, making cD a more informative signal for forensic analysis.

Effect of NPR. Building upon cD, we further examine the contribution of NPR. As shown in Table IV, incorporating NPR into ForeAgent slightly improves the overall accuracy from 72.41% to 73.03%, while also yielding a more balanced trade-off between real-image accuracy (95.26% vs. 96.12%) and fake-image accuracy (43.46% vs. 41.65%). This indicates that NPR provides complementary local statistical cues that enhance the model’s discriminative capability beyond what frequency-domain features alone can offer.

Based on these findings, we adopt cD combined with NPR as the default frequency-domain representation in ForeAgent.

2) *Effect of Iterations.*: Table 4 illustrates the impact of iteration numbers on model performance. The overall accuracy improves consistently from 73.03% (iteration 0) to **82.18%** (iteration 5), representing a gain of 9.15 percentage points. Notably, while Real Acc remains relatively stable around 95%-97% across all iterations, Fake Acc exhibits substantial improvement from 43.46% to 61.86%, an increase of 18.40 percentage points. This demonstrates that the self-evolution mechanism primarily enhances the model’s ability to detect fake news, which is typically the more challenging task, while maintaining robust performance on real news classification.

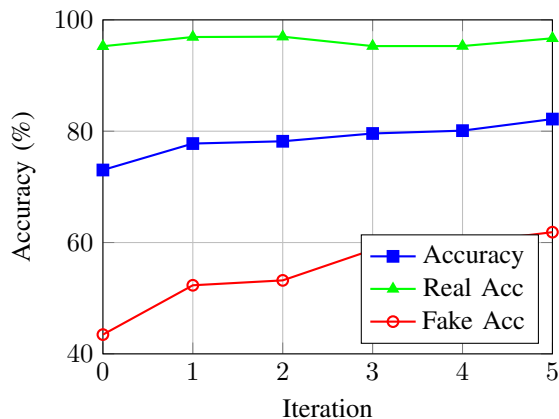


Fig. 4. Performance trends across iterations on Chameleon.

3) *The effect of Quality-Gating model.*: We adopt a dual-expert quality-gating module that combines ForeAgent (Qwen3-VL-8B) and Qwen3-VL-Plus, motivated by three con-

siderations: 1)**Complementarity**: As shown in Table V, the two individual models exhibit complementary strengths—the 8B model yields higher reasoning quality (4.53 vs. 4.36) owing to its shared architectural lineage with ForeAgent, which provides a consistent “internal” quality perspective on the generated rationales; the more capable Plus model achieves higher detection accuracy (92.2% vs. 91.5%) thanks to its stronger visual reasoning capabilities, offering a reliable “external” assessment. Their combination leverages both advantages, achieving the best accuracy **93.3%** and reasoning quality **5.12** simultaneously. 2)**Bias mitigation**: Relying solely on the 8B model to evaluate its own generations may introduce self-reinforcing biases, where the model systematically overlooks its own failure modes. The Plus model serves as an independent cross-validator, breaking this self-evaluation loop and enabling more objective quality assessment. 3)**Synergistic filtering**: A sample is retained only when *both* experts agree on its quality, enforcing a stricter consensus-based criterion that reduces the risk of low-quality rationales passing through either model’s blind spots. The dual-expert strategy improves accuracy by 1.8%/1.1% and reasoning quality by 13.0%/17.4% over the 8B-only and Plus-only baselines, respectively, confirming that the two experts provide genuinely complementary supervision signals.

TABLE V
COMPARING DIFFERENT QUALITY-GATING STRATEGIES ON AIGCDETECTBENCHMARK.

Gating Strategy	Accuracy	Reasoning Quality
Qwen3-VL-8B Only	91.5%	4.53
Qwen3-VL-Plus Only	92.2%	4.36
Dual-Expert (Ours)	93.3%	5.12

4) *Self-evolution vs. GPT-synthesized Supervision*: A natural question arises: can we simply leverage powerful LLMs to synthesize reasoning supervision for training? To investigate this, we construct a baseline where GPT5 is provided with images and ground-truth labels to generate reasoning processes, yielding 100K synthetic SFT samples. We then fine-tune the same pre-trained backbone on this dataset for fair comparison.

As shown in Table VI, while the GPT-synthesized SFT approach achieves a higher Fake Acc (69.62% vs. 61.86%), it substantially underperforms on Real Acc (90.07% vs. 96.69%) and overall accuracy (81.29% vs. 82.18%). More critically, the reasoning quality score is notably lower (4.44 vs. 5.35). These results reveal two key insights: (1) GPT-synthesized reasoning, despite being generated by a more powerful model, may introduce noise or hallucinations that degrade the model’s ability to correctly identify authentic content, leading to over-detection of fake news; (2) The self-evolution paradigm produces higher-quality reasoning traces that are better aligned with the model’s own capabilities, resulting in more reliable and balanced detection performance. This validates our design choice of adopting self-evolution over direct knowledge distillation from external LLMs.

TABLE VI
COMPARISON BETWEEN GPT-SYNTHESIZED SFT DATA AND
SELF-EVOLUTION PARADIGM.

Method	Real Acc	Fake Acc	Overall	Reasoning Score
Qwen3-VL-8B (GPT*)	90.07%	69.62%	81.29%	4.44
ForeAgent	96.69%	61.86%	82.18%	5.35

IV. OVERVIEW OF ERROR ANALYSIS ON AIGCDETECTBENCHMARK

We conduct error analysis on 65% of the misclassified samples (5,146 cases) from the AIGCDetectBenchmark test set. As shown in Table VII, the error distribution exhibits a significant imbalance: false negatives (Fake→Real) account for 86.82% (4,468 cases), vastly outnumbering false positives (Real→Fake) at 13.18% (678 cases). This 6.6:1 ratio reveals that the detection system fails primarily by missing fake images rather than by incorrectly flagging real ones, indicating a systematic bias toward classifying images as “real”, likely due to the high visual quality of modern generative models that successfully deceive the visual reasoning process.

TABLE VII
DISTRIBUTION OF ERROR TYPES

Error Type	Count	Percentage
False Negative (Fake→Real)	4,468	86.82%
False Positive (Real→Fake)	678	13.18%
Total	5,146	100%

A. Round 2 Flip Error Analysis

a) Reasoning Consistency Between Rounds.: We categorize all error samples based on the agreement between Round 1 and Round 2 predictions. Among the 5,146 errors, **1,450 samples (28.18%)** represent cases where Round 1 made the correct prediction but Round 2 incorrectly reversed it, while the remaining 3,696 cases (71.82%) are consistent errors across both rounds. This indicates that the second-round verification mechanism introduces a non-negligible number of new errors rather than purely correcting existing ones.

Further directional analysis of these 1,450 flip errors reveals an extreme asymmetry: 1,431 cases (98.66%) involve flipping correct “fake” predictions to incorrect “real,” while only 19 cases (1.34%) go in the opposite direction. This stark imbalance points to a systematic vulnerability in Round 2 that strongly favors “real” classifications. Moreover, when confidence scores increase from Round 1 to Round 2, 93.4% of such cases are false negatives, suggesting that the model becomes *more* confident in its incorrect “real” predictions during the review process, with an overall mean confidence of 0.9617 on misclassified samples.

b) Reasoning Patterns and Root Causes.: To understand why Round 2 incorrectly overturns correct predictions, we analyze the reasoning types and justifications employed in flip errors (Table VIII).

TABLE VIII
ROUND 2 REASONING PATTERNS IN FLIP ERRORS

Reasoning / Justification	Count	%
<i>Analysis Types Used by Round 2</i>		
Texture Analysis	1,275	87.9%
Lighting Analysis	1,249	86.1%
AI Artifact Claims	1,028	70.9%
Anatomical Analysis	714	49.2%
Physical Impossibility	82	5.7%
<i>Justifications for “Real” Classification</i>		
Overall Coherence	1,189	83.1%
Consistent Lighting	754	52.7%
Natural Texture	428	29.9%
Physical Plausibility	231	16.1%
Correct Anatomy	228	15.9%

The results reveal three root causes of Round 2 failures:

- 1) **Visual Appearance Bias:** Round 2 heavily relies on texture (87.9%) and lighting (86.1%) analysis—surface-level features that modern generators excel at synthesizing. The most common justification for overturning to “real” is “overall coherence” (83.1%), reflecting a *coherence fallacy*: the assumption that visual consistency implies authenticity.
- 2) **Frequency Domain Distrust:** In 87.3% of false negative flip cases, Round 2 expresses skepticism toward wavelet analysis, often dismissing frequency-domain evidence as “technical artifacts” rather than valid forensic signals. This leads Round 2 to override correct Round 1 judgments that were grounded in spectral cues.
- 3) **Overconfidence:** In the 0.98–1.00 confidence range, 97.7% of errors are false negatives, indicating severe miscalibration where the model is most confident precisely when it is wrong about “real” predictions.

c) Case Study.: We present two representative examples to illustrate both the failure and success modes of the dual-round reasoning mechanism. In Figure 5, Round 1 correctly identifies a fake portrait by detecting facial over-smoothing and wavelet anomalies, yet Round 2 overrides this judgment by attributing these artifacts to natural photographic conditions (soft lighting, bokeh), exemplifying the *coherence fallacy* and *frequency domain distrust* patterns. In contrast, Figure 6 demonstrates the intended benefit of dual-round verification: Round 1 over-interprets normal photographic features of a real street scene as AI-generation artifacts (a false alarm), while Round 2 correctly recognizes the scene’s authentic consistency and rectifies the initial misjudgment. Together, these two cases reveal that Round 2 succeeds when it leverages *holistic visual reasoning* to suppress false positives, but fails when it applies the same reasoning to dismiss valid *local forensic evidence*, inadvertently introducing false negatives that modern generators are specifically optimized to exploit.

V. RELATED WORK

The rapid proliferation of generative models, such as GANs and Diffusion Models, has made the identification of AI-generated images (AIGI) a pivotal challenge in digital forensics. Current research can be broadly categorized



Perception	Fake 0.95
Reasoning Facial skin exhibits unnaturally uniform smoothness without pores; water droplets on the jacket appear overly regular in size and distribution. Wavelet coefficients show abnormal high-frequency attenuation in facial regions; NPR map highlights irregular patterns along hair boundaries.	
Result: Fake ✓	
Verdict	Real 0.85
Reasoning Natural wet-hair rendering, coherent rainy-day lighting, and plausible depth-of-field blur. The “smoothness” is consistent with overcast soft lighting. Wavelet patterns are attributable to bokeh and JPEG compression, not generative artifacts.	
Result: Real ✗	

Fig. 5. Flip error case. Ground truth: **False**. During the perception round, ForeAgent correctly identifies AI-generation artifacts, but ForeAgent dismisses frequency-domain evidence in favor of visual coherence, incorrectly overriding to “Real” in the verdict round.



Perception	Fake 0.95
Reasoning Crowd reveals repetitive postures and spatial intervals; façades show misaligned windows; Chinese signage displays character-level distortions. Wavelet cD sub-band reveals abnormal high-frequency attenuation; NPR map highlights irregularities around pedestrian boundaries.	
Result: Fake ✗	
Verdict	Real 0.98
Reasoning Coherent commercial street with consistent perspective, natural crowd behavior, and plausible overcast lighting across architectural elements. Wavelet patterns appear within normal range, consistent with typical urban photography.	
Result: Real ✓	

Fig. 6. Successful correction case. During the perception round, ForeAgent over-interprets normal photographic characteristics as AI-generation artifacts, while ForeAgent correctly recognizes the scene’s authentic visual consistency and re-interprets frequency-domain patterns in the verdict stage.

into feature-based discriminative models and Large Vision-Language Model (LVLM) based explainable detectors.

a) *Feature-based detection*: Early methods [7]–[13] primarily utilized ResNet or ViT backbones to extract statistical artifacts. NPR rethink the generator architectures and identify structural traces left by up-sampling operations, proposing Neighboring Pixel Relationships as a generalizable feature. To address the limitations of single-modality features, AIDE employs a mixture-of-experts approach, combining semantic embeddings from OpenCLIP with low-level frequency patterns derived from DCT scoring and SRM filters. Furthermore, Effort [11] identifies the “asymmetry phenomenon” where models overfit to monotonous fake patterns; it utilizes Singular Value Decomposition (SVD) to decompose the feature space into orthogonal semantic and forgery subspaces, thereby preserving pre-trained knowledge while enhancing generalization. However, these methods often treat detection as a “black-box” binary classification, lacking logical transparency.

b) *MLLMs-based detection*: The integration of MLLMs [14]–[19] has opened a new frontier for interpretable forensics. AIGI-Holmes couples LLaVA with low-level experts (e.g., NPR) and utilizes a three-stage pipeline (visual pre-training, SFT, and DPO) to provide human-verifiable explanations. Similarly, FakeShield and SIDA extend the task to include tampered region localization and conversational interaction. Regarding reasoning logic, FakeReasoning introduces a structured Chain-of-Thought (CoT) to decompose the reasoning

process into summary, caption, reasoning, and conclusion stages. Despite their progress, existing MLLMs-based methods often rely on static fine-tuning datasets and lack a mechanism for iterative self-correction.

VI. CONCLUSION

In this paper, we introduced **ForeAgent**, an agentic forensic framework for AI-generated image detection that addresses two key limitations of existing MLLM-based approaches: insufficient sensitivity to fine-grained artifacts and heavy reliance on proprietary models or costly expert annotations. ForeAgent employs a *Perception–Verdict* architecture to integrate semantic, spatial, and frequency-domain cues, producing coherent and logically grounded decisions via an MLLM-based verdict module. To enable continual self-improvement without human supervision, we proposed a *Hindsight-Driven Self-Refining* mechanism that iteratively reflects on erroneous predictions and applies dual-expert quality gating to curate high-quality fine-tuning samples. Extensive experiments validate the effectiveness of our approach. On the Chameleon benchmark, ForeAgent achieves state-of-the-art accuracy of 82.18%, surpassing AIDE by 16.41%. On AIGCDetectBenchmark, it attains 93.3% mean accuracy across 16 diverse generators. Qualitative evaluations further show that ForeAgent’s interpretable reasoning exceeds that of GPT-5, highlighting the value of hindsight-driven self-refinement for both detection and explainability.

Limitations and Future Work. Despite strong overall performance, ForeAgent shows reduced accuracy on certain sources with distinct characteristics (e.g., WFIR), suggesting that source-specific augmentation or improved spatial-frequency modeling may help. The current framework also relies on a fixed set of multi-view features; adaptive or learnable feature selection could further enhance robustness. Moreover, the iterative hindsight-driven refinement paradigm is naturally compatible with reinforcement learning. Future work will explore online RL-based strategies for continuous, real-time adaptation to improve efficiency and generalization. We also plan to extend the framework beyond binary real/fake classification to broader forensic tasks, including fine-grained manipulation localization and multi-source attribution.

ACKNOWLEDGMENTS

This work was supported in part by the National Natural Science Foundation of China (NSFC) under Grant No. U24A20326 (Regional Joint Fund Project: “Theory and Methods of Cloud-Edge Collaborative Lightweight Autonomous Intelligent Computing for Content Generation Scenarios,” 2025–2028).

REFERENCES

- [1] I. J. Goodfellow, J. Pouget-Abadie, M. Mirza, B. Xu, D. Warde-Farley, S. Ozair, A. Courville, and Y. Bengio, “Generative adversarial nets,” in *Advances in Neural Information Processing Systems*, Z. Ghahramani, M. Welling, C. Cortes, N. Lawrence, and K. Weinberger, Eds., vol. 27. Curran Associates, Inc., 2014. [Online]. Available: https://proceedings.neurips.cc/paper_files/paper/2014/file/f033ed80deb0234979a61f95710dbe25-Paper.pdf
- [2] J. Ho, A. Jain, and P. Abbeel, “Denosing diffusion probabilistic models,” in *Proceedings of the 34th International Conference on Neural Information Processing Systems*, ser. NIPS ’20. Red Hook, NY, USA: Curran Associates Inc., 2020.
- [3] T. Li, Y. Tian, H. Li, M. Deng, and K. He, “Autoregressive image generation without vector quantization,” in *The Thirty-eighth Annual Conference on Neural Information Processing Systems*, 2024. [Online]. Available: <https://openreview.net/forum?id=VNBIF0gmkb>
- [4] K. Tian, Y. Jiang, Z. Yuan, B. PENG, and L. Wang, “Visual autoregressive modeling: Scalable image generation via next-scale prediction,” in *The Thirty-eighth Annual Conference on Neural Information Processing Systems*, 2024. [Online]. Available: <https://openreview.net/forum?id=goJL67CfS8>
- [5] M. Huh, A. Liu, A. Owens, and A. A. Efros, “Fighting fake news: Image splice detection via learned self-consistency,” in *Proceedings of the European Conference on Computer Vision (ECCV)*, September 2018.
- [6] J. Ren, H. Xu, P. He, Y. Cui, S. Zeng, J. Zhang, H. Wen, J. Ding, P. Huang, L. Lyu, H. Liu, Y. Chang, and J. Tang, “Copyright protection in generative ai: A technical perspective,” 2024. [Online]. Available: <https://arxiv.org/abs/2402.02333>
- [7] S. McCloskey and M. Albright, “Detecting gan-generated imagery using saturation cues,” in *2019 IEEE International Conference on Image Processing (ICIP)*, 2019, pp. 4584–4588.
- [8] S.-Y. Wang, O. Wang, R. Zhang, A. Owens, and A. A. Efros, “Cnn-generated images are surprisingly easy to spot...for now,” in *CVPR*, 2020.
- [9] J. Frank, T. Eisenhofer, L. Schönherr, A. Fischer, D. Kolossa, and T. Holz, “Leveraging frequency analysis for deep fake image recognition,” in *Proceedings of the 37th International Conference on Machine Learning*, ser. ICML’20. JMLR.org, 2020.
- [10] T. Karras, T. Aila, S. Laine, and J. Lehtinen, “Progressive growing of GANs for improved quality, stability, and variation,” in *International Conference on Learning Representations*, 2018. [Online]. Available: <https://openreview.net/forum?id=Hk99zCeAb>
- [11] Z. Yan, J. Wang, P. Jin, K.-Y. Zhang, C. Liu, S. Chen, T. Yao, S. Ding, B. Wu, and L. Yuan, “Orthogonal subspace decomposition for generalizable AI-generated image detection,” in *Forty-second International Conference on Machine Learning*, 2025. [Online]. Available: <https://openreview.net/forum?id=GFpjO8S8Po>
- [12] C. Tan, H. Liu, Y. Zhao, S. Wei, G. Gu, P. Liu, and Y. Wei, “Rethinking the up-sampling operations in cnn-based generative network for generalizable deepfake detection,” 2023.
- [13] S. Yan, O. Li, J. Cai, Y. Hao, X. Jiang, Y. Hu, and W. Xie, “A sanity check for AI-generated image detection,” in *The Thirteenth International Conference on Learning Representations*, 2025. [Online]. Available: <https://openreview.net/forum?id=ODRHZrkOQM>
- [14] Z. Huang, J. Hu, X. Li, Y. He, X. Zhao, B. Peng, B. Wu, X. Huang, and G. Cheng, “SIDA: social media image deepfake detection, localization and explanation with large multimodal model,” in *IEEE/CVF Conference on Computer Vision and Pattern Recognition (CVPR) 2025*, 2025.
- [15] Y. Gao, D. Chang, B. Yu, H. Qin, M. Diao, L. Chen, K. Liang, and Z. Ma, “Towards generalizable forgery detection and reasoning,” 2025. [Online]. Available: <https://arxiv.org/abs/2503.21210>
- [16] X. Yang and J. Zhou, “Research about the ability of llm in the tamper-detection area,” 2024. [Online]. Available: <https://arxiv.org/abs/2401.13504>
- [17] Y. Zhang, B. Colman, X. Guo, A. Shahriyari, and G. Bharaj, “Common sense reasoning for deepfake detection,” 2024. [Online]. Available: <https://arxiv.org/abs/2402.00126>
- [18] Z. Zhou, Y. Luo, Y. Wu, K. Sun, J. Ji, K. Yan, S. Ding, X. Sun, Y. Wu, and R. Ji, “Aigi-holmes: Towards explainable and generalizable ai-generated image detection via multimodal large language models,” *arXiv preprint arXiv:2507.02664*, 2025.
- [19] H. Kang, S. Wen, Z. Wen, J. Ye, W. Li, P. Feng, B. Zhou, B. Wang, D. Lin, L. Zhang *et al.*, “Legion: Learning to ground and explain for synthetic image detection,” *arXiv preprint arXiv:2503.15264*, 2025.
- [20] P. Agrawal, S. Antoniak, E. B. Hanna, B. Bout, D. Chaplot, J. Chudnovsky, D. Costa, B. D. Monicault, S. Garg, T. Gervet, S. Ghosh, A. Héliou, P. Jacob, A. Q. Jiang, K. Khandelwal, T. Lacroix, G. Lample, D. L. Casas, T. Lavril, T. L. Scao, A. Lo, W. Marshall, L. Martin, A. Mensch, P. Muddireddy, V. Nemychnikova, M. Pellat, P. V. Platen, N. Raghuraman, B. Rozière, A. Sablayrolles, L. Saulnier, R. Sauvestre, W. Shang, R. Soletskiy, L. Stewart, P. Stock, J. Studnia, S. Subramanian, S. Vaze, T. Wang, and S. Yang, “Pixtral 12b,” 2024. [Online]. Available: <https://arxiv.org/abs/2410.07073>
- [21] Z. Xu, X. Zhang, R. Li, Z. Tang, Q. Huang, and J. Zhang, “Fakeshield: Explainable image forgery detection and localization via multi-modal large language models,” in *International Conference on Learning Representations*, 2025.
- [22] OpenAI, “Gpt-4o system card,” 2024. [Online]. Available: <https://arxiv.org/abs/2410.21276>
- [23] Y. Ju, S. Jia, L. Ke, H. Xue, K. Nagano, and S. Lyu, “Fusing global and local features for generalized ai-synthesized image detection,” in *2022 IEEE International Conference on Image Processing (ICIP)*, 2022, pp. 3465–3469.
- [24] B. Liu, F. Yang, X. Bi, B. Xiao, W. Li, and X. Gao, “Detecting generated images by real images,” in *Computer Vision – ECCV 2022*, S. Avidan, G. Brostow, M. Cissé, G. M. Farinella, and T. Hassner, Eds. Cham: Springer Nature Switzerland, 2022, pp. 95–110.
- [25] C. Tan, Y. Zhao, S. Wei, G. Gu, and Y. Wei, “Learning on gradients: Generalized artifacts representation for gan-generated images detection,” in *Proceedings of the IEEE/CVF Conference on Computer Vision and Pattern Recognition*, 2023, pp. 12 105–12 114.
- [26] Z. Wang, J. Bao, W. Zhou, W. Wang, H. Hu, H. Chen, and H. Li, “Dire for diffusion-generated image detection,” in *Proceedings of the IEEE/CVF International Conference on Computer Vision (ICCV)*, October 2023, pp. 22 445–22 455.
- [27] U. Ojha, Y. Li, and Y. J. Lee, “Towards universal fake image detectors that generalize across generative models,” in *CVPR*, 2023.
- [28] N. Zhong, Y. Xu, S. Li, Z. Qian, and X. Zhang, “Patchcraft: Exploring texture patch for efficient ai-generated image detection,” 2024. [Online]. Available: <https://arxiv.org/abs/2311.12397>
- [29] Q. Team, “Qwen3-vl technical report,” 2025. [Online]. Available: <https://arxiv.org/abs/2511.21631>
- [30] M. Zhu, H. Chen, Q. YAN, X. Huang, G. Lin, W. Li, Z. Tu, H. Hu, J. Hu, and Y. Wang, “Genimage: A million-scale benchmark for detecting ai-generated image,” in *Advances in Neural Information Processing Systems*, A. Oh, T. Naumann, A. Globerson, K. Saenko, M. Hardt, and S. Levine, Eds., vol. 36. Curran Associates, Inc., 2023, pp. 77 771–77 782. [Online]. Available: https://proceedings.neurips.cc/paper_files/paper/2023/file/f4d4a021f9051a6c18183b059117e8b5-Paper-Datasets_and_Benchmarks.pdf